and transistors already in use in electronics. We note that room temperature ferromagnetism in semiconductors has been predicted[10]. Combinations of semiconductor spintronic devices[17,18] with the present field-controlled ferromagnetism may also be important in quantum information technologies that are based on manipulation of spin states in semiconductors[19,20]. □

Received 5 September; accepted 1 November 2000.

1. Prinz, G. A. Magnetoelectronics. *Science* **282,** 1660–1663 (1998).
2. de Boeck, J. & Borghs, G. Magnetoelectronics. *Phys. World* **12,** 27–32 (1999).
3. Ohno, H., Munekata, H., Penney, T., von Molnár, S. & Chang, L. L. Magnetotransport properties of p-type (In,Mn)As diluted magnetic III-V semiconductors. *Phys. Rev. Lett.* **68,** 2664–2667 (1992).
4. Munekata, H., Zaslavsky, A., Fumagalli, P. & Gambino, R. J. Preparation of (In,Mn)As/(Ga,Al)Sb magnetic semiconductor heterostructures and their ferromagnetic characteristics. *Appl. Phys. Lett.* **63,** 2929–2931 (1993).
5. Ohno, H. Making nonmagnetic semiconductors ferromagnetic. *Science* **281,** 951–956 (1998).
6. Ohno, H. Properties of ferromagnetic III-V semiconductors. *J. Mag. Magn. Mater.* **200,** 110–129 (1999).
7. Koshihara, S. *et al.* Ferromagnetic order induced by photogenerated carriers in magnetic III-V semiconductor heterostructures of (In,Mn)As/GaSb. *Phys. Rev. Lett.* **78,** 4617–4620 (1997).
8. Munekata, H. *et al.* Diluted magnetic III-V semiconductors. *Phys. Rev. Lett.* **63,** 1849–1852 (1989).
9. Soo, Y. L., Huang, S. W., Ming, Z. H., Kao, Y. H. & Munekata, H. III-V diluted magnetic semiconductor: Substitutional doping of Mn in InAs. *Phys. Rev. B* **53,** 4905–4909 (1996).
10. Dietl, T., Ohno, H., Matsukura, F., Cibert, J. & Ferrand, D. Zener model description of ferromagnetism in zinc-blende magnetic semiconductors. *Science* **287,** 1019–1022 (2000).
11. von Molnár, S., Munekata, H., Ohno, H. & Chang, L. L. New diluted magnetic semiconductor based on III-V compounds. *J. Mag. Magn. Mater.* **93,** 356–364 (1991).
12. Shen, A. *et al.* Epitaxy and properties of InMnAs/AlGaSb diluted magnetic III-V semiconductor heterostructures. *Appl. Surf. Sci.* **113/114** 183–188 (1997).
13. Chien, C. L. & Westgate, C. W. *The Hall Effect and Its Applications* 43–51 (Plenum, New York, 1980).
14. Arrott, A. Criterion for ferromagnetism from observations of magnetic isotherms. *Phys. Rev.* **108,** 1394–1395 (1957).
15. Dietl, T., Haury, A. & Merle d'Aubigné, Y. Free carrier-induced ferromagnetism in structures of diluted magnetic semiconductors. *Phys. Rev. B* **55,** R3347–R3350 (1997).
16. Lee, B., Jungwirth, T. & MacDonald, A. H. Theory of ferromagnetism in diluted magnetic semiconductor quantum wells. *Phys. Rev. B* **61,** 15606–15609 (2000).
17. Fiederling, R. *et al.* Injection and detection of a spin-polarized current in a light-emitting diode. *Nature* **402,** 787–790 (1999).
18. Ohno, Y. *et al.* Electrical spin injection in a ferromagnetic semiconductor heterostructure. *Nature* **402,** 790–792 (1999).
19. Loss, D. & DiVincenzo, D. P. Quantum computation with quantum dots. *Phys. Rev. A* **57,** 120–126 (1998).
20. Vrijen, R. *et al.* Electron-spin-resonance transistors for quantum computing in silicon-germanium heterostructures. *Phys. Rev. A* **62,** 012306-1–10 (2000).

Acknowledgements

This work was supported by the Japan Society for the Promotion of Science, the Ministry of Education, Japan, and the Mitsubishi Foundation.

Correspondence and requests for materials should be addressed to H.O. (e-mail: ohno@riec.tohoku.ac.jp).

Mesoscopic fast ion conduction in nanometre-scale planar heterostructures

N. Sata, K. Eberman*, K. Eberl & J. Maier

Max-Planck-Institut für Festkörperforschung, 70569 Stuttgart, Germany

Ion conduction is of prime importance for solid-state reactions in ionic systems, and for devices such as high-temperature batteries and fuel cells, chemical filters and sensors[1,2]. Ionic conductivity in solid electrolytes can be improved by dissolving appropriate impurities into the structure or by introducing interfaces that cause the redistribution of ions in the space-charge regions[3–11]. Heterojunctions in two-phase systems should be particularly efficient at improving ionic conduction[3,4], and a qualitatively different conductivity behaviour is expected when interface spacing is comparable to or smaller than the width of the space-charge regions in comparatively large crystals[12–15]. Here we report the preparation, by molecular-beam epitaxy, of defined hetero-layered films composed of CaF_2 and BaF_2 that exhibit ionic conductivity (parallel to the interfaces) increasing proportionally with interface density—for interfacial spacing greater than 50 nanometres. The results are in excellent agreement with semi-infinite space-charge calculations[3], assuming a redistribution of fluoride ions at the interfaces. If the spacing is reduced further, the boundary zones overlap and the predicted mesoscopic size effect[3,12] is observed. At this point, the single layers lose their individuality and an artificial ionically conducting material with anomalous transport properties is generated. Our results should lead to fundamental insight into ionic contact processes and to tailored ionic conductors of potential relevance for medium-temperature applications.

The growth of semiconductor heterostructures by molecular beam epitaxy (MBE) is the method of choice for preparing hetero-systems with highly defined geometry, periodicity, interfacial spacings and layer sequence[16,17]. We used this technique, performed in a high-vacuum chamber with a base pressure of 10^{-9} mbar. Single crystals of the moderate (anti-Frenkel disordered) fluoride conductors CaF_2 and BaF_2 (refs 18–20) were sublimed at 1,180 and 1,000 °C, respectively, leading to a layer growth rate of about 1 nm min^{-1}. Periodicity and thickness were varied over a wide range (individual layer thicknesses: 2–500 nm) by computer-controlled effusion cell shutters. The total thickness of the film packages ranged from 200 to 500 nm. Single crystals of Al_2O_3 and SiO_2 were tested as substrate materials; they showed little influence on the conductivity of the thin films, whereas they obviously affected crystallinity. The substrate was kept at a temperature of 500 °C or about 100 °C to investigate the effect of growth temperature on film structure, which could also affect the ionic conductivity.

The films were characterized by X-ray diffraction and secondary-ion mass spectrometry (SIMS). In contrast to CaF_2, the BaF_2 film grows on Al_2O_3(012) substrates at a temperature of 500 °C in [111]

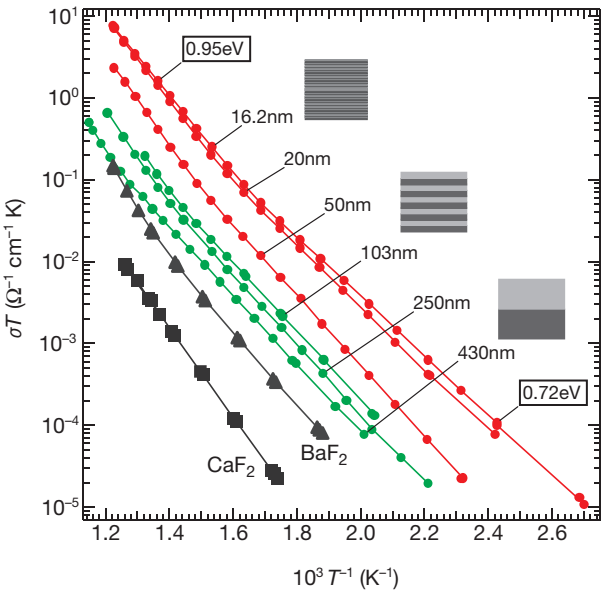

Figure 1 Parallel ionic conductivity of the films. Data are shown for films with various periods and interfacial densities in the 430–16 nm range. We note that the overall thickness is approximately the same in all cases (~500 nm). σ, conductivity; T, temperature. The different colours refer to different site regimes (green: semi-infinite space charge zones; red: finite space charge zones).

* Present address: 3M Center, St Paul, Minnesota 55144-1000, USA.

directions exclusively. Therefore, BaF_2 was deposited as the first layer. Such heterolayered films exhibited a uniform crystal orientation when prepared at high substrate temperatures (that is, about 500 °C), as confirmed by X-ray pole-figure measurements, and by transmission electron microscopy (TEM). Films obtained at low substrate temperatures (about 100 °C), or obtained from simultaneous BaF_2 and CaF_2 beams, are polycrystalline.

The SIMS spectra of the BaF_2/CaF_2 heterofilms showed clearly the layered character of the structure with minor mutual solubility. Although we detected oxygen and carbon impurities by SIMS, the fact that their amount did not vary strongly between the different samples excludes any major relevance to the effects considered. While TEM shows rather sharp boundaries, a certain degree of intermixing of Ba and Ca at the interface cannot be ruled out by the SIMS measurements, owing to the limited resolution.

Platinum films were deposited on the surface of the heterostructure as rectangular-shaped electrodes for lateral conductivity measurements. The 13-mm-long surface electrodes were separated by 1 mm, which may be compared with the film thicknesses of less than 10^{-3} mm. This geometry ensures that the parallel conductance of the total film was measured. Ionic conductivities were confirmed by impedance spectra, obtained by a.c. impedance measurements from 1 to 10^4 Hz at different temperatures over the range 540–100 °C.

The results for the pure CaF_2 and BaF_2 films (black symbols in Fig. 1) show the intrinsic to extrinsic transition, as in the bulk, with the expected activation energies. But owing to the small sample thickness (~500 nm), the low-temperature conductivity need not, at least not exclusively, be due to impurity doping (for example, O^{2-} on F^- sites), as the space-charge contribution of the surface and the substrate interface would result in similar slopes[9,12,21]. (We note the similarity of the BaF_2 data to the results of calculations involving two space-charge layers, which will be discussed below.)

Figures 1 and 2 reveal that large conductivities can be achieved in the heterostructures. The examples given there are …CaF_2/BaF_2… heterolayers composed of CaF_2 and BaF_2 units of uniform and equal thicknesses, with varying interfacial densities while the overall film thickness L was always similar (470 ± 40 nm).

All experimental results shown in Fig. 1 are stationary values observed after annealing at 540 °C. The first cycles suffer from non-equilibrium effects possibly due to non-stationary dislocations. The heterolayers show conductivities that are higher than those of pure CaF_2 or BaF_2 films (and also higher than that of $(Ba,Ca)F_2$). The conductivity increases progressively with increasing interfacial density (decreasing period) in the period range 500 to 16 nm (here period refers to the thickness of CaF_2 plus BaF_2 unit layer). The change of conductivity with temperature is the same as expected for composite electrolytes[3]: at low temperature there is a conductivity enhancement characterized by an activation energy close to the migration enthalpy of the relevant carriers. In the heterogeneously doped solid electrolytes, this enhancement was attributed to a space-charge layer with an enhanced carrier concentration and an almost temperature-independent interfacial concentration.

Provided that the period is greater than ~100 nm, the conductivity increases linearly with N/L (Fig. 2); that is, approximately linearly with the number of heterojunctions N. The space-charge calculation[3,11] (the details of which are beyond the scope of this Letter) uses published data on defect formation and mobilities[18,19], and sets the interfacial concentration equal to the inverse molar volume[3]; even though performed without any adjustable parameter, it yields surprisingly good agreement with the experiments (see dotted line in Figs 2 and 3). A perfect agreement is obtained when the data are background-corrected (that is, when contributions that are not due to the variable number of heterojunctions—such as contributions from bulk, surface and substrate interface—are accounted for), as shown by the bold lines in Figs 2 and 3. The evaluation of the data indicates that, at lower temperature, the space-charge layers in BaF_2 are determining the overall conductivity (compare the migration enthalpy of 0.75 eV). This is in agreement with the higher mobilities in BaF_2 compared with CaF_2 at these comparatively low temperatures. Owing to the similarity of the

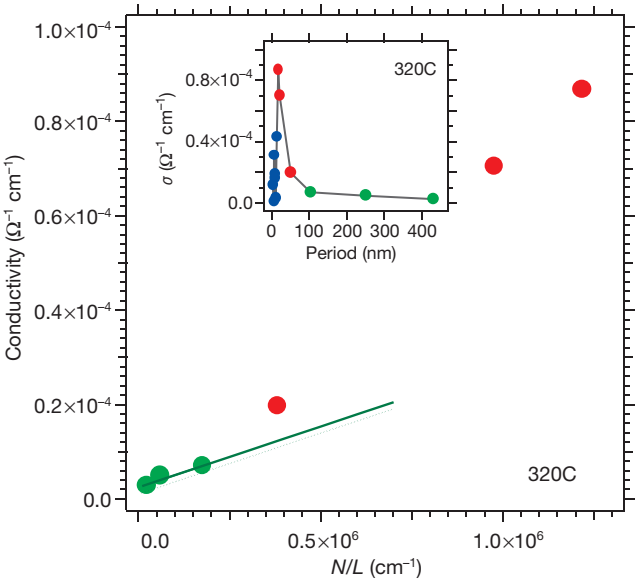

Figure 2 Variation of ionic conductivity with N/L. In the period range 430–100 nm (green), the (parallel) ionic conductivity increases monotonically with the number of interfaces (N). The linear increase with N/L (where L is overall thickness) exhibits exactly the slope obtained from the space-charge calculations. The prediction without any adjustable parameter (that is, ignoring background effects; dotted line) is very close to the absolute values. The bold line refers to the background-corrected calculation (red). The inset gives the conductivities as a function of the period in the range 430–2 nm. The samples with smaller spacings (blue) (~50 nm ≥ period ≥ 16 nm) show a further anomalous increase attributable to overlapping space charges. When the period is less than 16 nm (see inset), the conductivity decreases as discussed in the text.

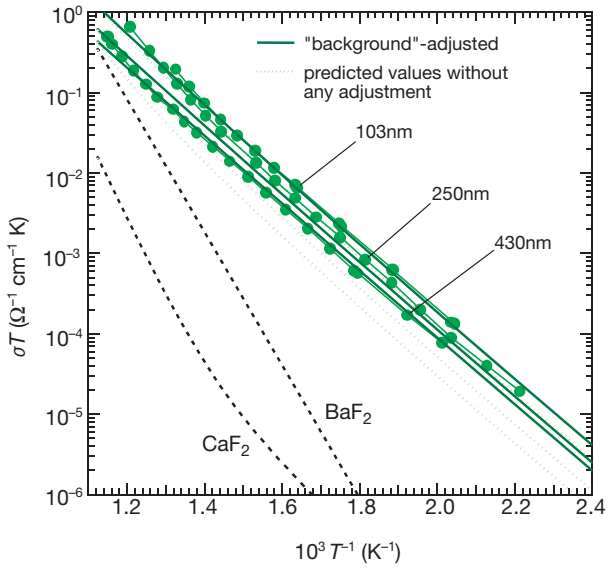

Figure 3 Comparison with space-charge calculations of the (parallel) conductivity results for the long-period films (green). Dotted lines, space-charge prediction with no background correction; solid lines, which perfectly agree with the experimental results (symbols), background-corrected. Dashed lines, the calculated intrinsic fluoride ion conductivities.

mobilities of interstitials and vacancies[18] in BaF_2, further conclusions about the mechanism cannot be drawn at this stage (but see below).

Figure 2 also shows that the conductivities obtained for periods smaller than 100 nm (and greater than 15 nm) are distinctly larger than those estimated for semi-infinite boundary conditions. The critical spacing (half period) separating the regime of semi-infinite space-charge effects from the mesoscopic regime of overlapping space charges has been derived to be 4λ (ref. 12), λ being the Debye length. Indeed a Debye length of about 10 nm is, in view of the extrinsic–intrinsic transition of the pure materials, approximately what we had expected. Thus, the anomalous increase at periods less than 100 nm (that is, spacing less than 50 nm) strongly suggests the appearance of the searched-for nanosize effect. The nanosize factor derived in refs 3 and 12—which takes account of this additional increase by the overlap of space-charge layers—is comparable with the value obtained from our data. As long as the defect concentration in the film centre is still markedly smaller than at the interface, the nanosize factor is roughly given by $4\lambda/l$, where l is the interfacial spacing. For $l = 8$ nm and $\lambda \approx 10$ nm, we expect it to be about 5, which is to be compared with Fig. 2. Even the hyperbolic dependence on l is reflected by the data in Fig. 2 inset, yielding an improved and consistent Debye length of 15 nm. The detailed space-charge calculation is extremely involved and cannot be given here (N.S. and J.M., manuscript in preparation).

A further reduction of the period below about 15 nm yielded a conductivity decrease (see Fig. 2 inset). On the one hand, this is indeed theoretically expected for extremely thin films[15] from the increased core–core interaction; on the other hand, however, the films are probably no longer continuous at these tiny thicknesses. Owing to the fact that the data start scattering (with respect to the l-dependence) at these extreme values, we now favour the second explanation.

We now consider the origin of the change in the activation energy of the short-period heterolayer samples at high temperatures in Fig. 1 (which differs in slope and onset temperature distinctly from the intrinsic bulk regime in the long-period heterolayer samples). An impurity effect would not be compatible with the space-charge considerations given here. Rather than being due to increasing conductivity of the core charge or to premelting effects, it seems that the more steeply activated CaF_2 space-charge conductivity determines the behaviour in this regime. Not only is the activation energy of 0.95 eV almost identical to the migration energy of F^- interstitials in CaF_2 (ref. 19), but also the dominating contribution of the CaF_2 layers is an automatic result of the quantitative treatment (N.S. and J.M., manuscript in preparation). (We note that the nanosize factor approximated by $4\lambda/l$ does not depend on temperature as long as the bulk is extrinsic.) If this is the correct explanation, a transfer of F^- from BaF_2 to CaF_2 is indicated, rather than a bilateral segregation of F^- to the interfacial core. The latter would also be not unexpected, as it would reduce the misfit strain. Whether this is indeed negligible—and to what degree the effects are influenced by interfacial mixing and to what extent further phenomena are involved—will need to be clarified in future studies.

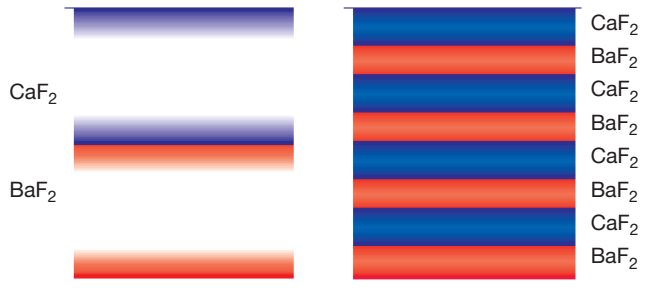

Figure 4 Comparison of conductivity profiles in the semi-infinite space-charge and mesoscale situations. The concentration or (parallel) conductivity profiles are sketched for the semi-infinite space-charge situation (period $> 8\lambda$, left), and for the mesoscale situation (period $< 8\lambda$, right) in which the space-charge regions overlap and bulk values are exceeded even in the centres of the individual layers.

Figure 4 displays the space-charge effects, which quantitatively account for the conductivity effects: it shows the semi-infinite space-charge situation as well as the mesoscopic situation in which there is no longer electro-neutral bulk. In the latter case, the layers have lost their individuality and an ensemble has formed with qualitatively new conductivity properties.

Our results open the way to the preparation of unusual artificial ion conductors and to the investigation of ionically conducting systems. Not only can interfacial effects be studied and used in high concentrations, but also mesoscopic phenomena can be explored—as shown here. The latter are important for potential applications in which a high conductivity normal to the interfaces is needed. Further systems of interest are: …MX/MX… layers with intentionally modified boundaries; …MX/A/MX… systems in which A represents a surface-active insulator; and heterolayers with mixed conductors in which both ionic and electronic conductivities are present. We expect the last of these systems to be of particular significance, because length scales determining size effects are different for electronic and ionic carriers. Whereas the effects discussed above are purely electrostatic in nature, we note that the standard term in the chemical potential of ionic defects changes if the structure changes[15]. For electrons, owing to their wave character and the related effective extension, such a size effect should occur on a much larger length scale. Like nano-electronics, the field of nano-ionics[15,21–23] relies on the metastability of the phase distribution and is characterized by a high information content on a mesoscopic scale. Both fields deserve further intensive exploration by advanced methods such as the one presented here. □

Received 7 August; accepted 18 October 2000.

1. Wagner, C. & Schottky, W. Theorie der geordneten Mischphasen. *Z. Phys. Chem. B* **11,** 163–210 (1930).
2. Kudo, T. & Fueki, K. *Solid State Ionics* 1st edn (VCH, Weinheim, 1990).
3. Maier, J. Ionic conduction in space charge regions. *Prog. Solid State Chem.* **23,** 171–263 (1995).
4. Maier, J. Space charge regions in solid two phase systems and their conduction contribution - II: contact equilibrium at the interphase of two ionic conductors and the related conductivity effect. *Ber. Bunsenges. Phys. Chem.* **89,** 355–362 (1985).
5. Maier, J. Defect chemistry and conductivity effects in heterogeneous solid electrolytes. *J. Electrochem. Soc.* **134,** 1524–1535 (1987).
6. Liang, C. C. Conduction characteristics of the lithium iodide-aluminum oxide solid electrolytes. *J. Electrochem. Soc.* **120,** 1289–1292 (1973).
7. Maier, J. Space charge regions in solid two phase systems and their conduction contribution - I. conductance enhancement in the system ionic conductor-'inert' phase and application on AgCl:Al_2O_3 and AgCl:SiO_2. *J. Phys. Chem. Solids* **46,** 309–320 (1985).
8. Maier, J., Lauer, U. & Göpel, W. Gas-sensitivity of AgCl interfaces. *Solid State Ionics* **40/41,** 463–467 (1990).
9. Saito, Y. & Maier, J. Ionic conductivity enhancement of the fluoride conductor CaF_2 by grain boundary activation using Lewis acids. *J. Electrochem. Soc.* **142,** 3078–3083 (1995).
10. Shahi, K. & Wagner, J. B. Fast ion-transport in silver-halide solid-solutions and multiphase systems. *Appl. Phys. Lett.* **37,** 757–759 (1980).
11. Maier, J. Enhancement of the ionic conductivity in solid-solid-dispersions by surface induced defects. *Ber. Bunsenges. Phys. Chem.* **88,** 1057–1062 (1984).
12. Maier, J. Space charge regions in solid two phase systems and their conduction contribution - III: defect chemistry and ionic conductivity in thin films. *Solid State Ionics* **23,** 59–67 (1987).
13. Maier, J. Point-defect thermodynamics and size effects. *Solid State Ionics* **131,** 13–22 (2000).
14. Lee, J. -S., Adams, S. & Maier, J. Transport and phase transition characteristics in AgI : Al_2O_3 composite electrolytes - Evidence for a highly conducting 7-layer AgI polytype. *J. Electrochem. Soc.* **147,** 2407–2418 (2000).
15. Maier, J. Point defect thermodynamics: Macro- vs. nanocrystals. *Electrochemistry* **68,** 395–402 (2000).
16. Eberl, K., Petroff, P. M. & Demeester, P. (eds) in *Proc. NATO Advanced Res. Workshop* (Kluwer, Dordrecht, 1995)
17. Farrow, R. F. C., Sullivan, P. W., Williams, G. M., Jones, G. R. & Cameron, D. C. MBE-grown fluoride films-a new class of epitaxial dielectrics. *J. Vac. Sci. Technol.* **19,** 415–420 (1981).
18. Bollmann, W. Ionic conductivity of pure and doped BaF_2 crystals. *Phys. Status Solidi A* **18,** 313–321 (1973).
19. Bollmann, W. & Reimann, R. Concentration and mobility of interstitial fluorine ions in CaF_2. *Phys. Status Solidi A* **16,** 187–196 (1973).
20. Schoonman, J. in *Fast Ion Transport in Solids* (eds Vashishta, P., Mundy, V & Shenoy, V) 631–636 (Elsevier, North-Holland, New York, 1979).

21. Puin, W., Rodewald, S., Ramlau, R., Heitjans, P. & Maier, J. Local and overall ionic conductivity in nanocrystalline CaF_2. *Solid State Ionics* **131,** 159–164 (2000).
22. Schoonman, J. Nanostructured materials in solid state ionics. *Solid State Ionics* **135–137,** 5–20 (2000).
23. Tuller, H. L. Ionic conduction in nanocrystalline materials. *Solid State Ionics* **131,** 143–157 (2000).

Acknowledgements

We thank W. Kussmaul for experimental assistance, G. Bilger and H. Kerber for the performance of SIMS and X-ray pole-figure measurements, and W. Dietsche for advice.

Correspondence and requests for materials should be addressed to J.M. (e-mail: weiglein@chemix.mpi-stuttgart.mpg.de) or to U.S. (e-mail: sata@chemix.mpi-stuttgart.mpg.de).

Pairing of isolated nucleic-acid bases in the absence of the DNA backbone

Eyal Nir*, Karl Kleinermanns† & Mattanjah S. de Vries*‡

* *Department of Chemistry, The Hebrew University of Jerusalem, Jerusalem 91904, Israel*
† *Institut für Physikalische Chemie und Elektrochemie, Heinrich Heine Universität, D-40225 Düsseldorf, Germany*
‡ *Department of Chemistry and Biochemistry, University of California, Santa Barbara, California 93106, USA*

The two intertwined strands of DNA are held together through base pairing—the formation of hydrogen bonds between bases located opposite each other on the two strands. DNA replication and transcription involve the breaking and re-forming of these hydrogen bonds, but it is difficult to probe these processes directly. For example, conventional DNA spectroscopy[1–3] is dominated by solvent interactions, crystal modes and collective modes of the DNA backbone; gas-phase studies, in contrast, can in principle measure interactions between individual molecules in the absence of external effects, but require the vaporization of the interacting species without thermal degradation[4–9]. Here we report the generation of gas-phase complexes comprising paired bases, and the spectroscopic characterization of the hydrogen bonding in isolated guanine–cytosine (G–C) and guanine–guanine (G–G) base pairs. We find that the gas-phase G–C base pair adopts a single configuration, which may be Watson–Crick, whereas G–G exists in two different configurations, and we see evidence for proton transfer in the G–C pair, an important step in radiation-induced DNA damage pathways[10]. Interactions between different bases and between bases and water molecules can also be characterized by our approach, providing stringent tests for high-level *ab initio* computations that aim to elucidate the fundamental aspects of nucleotide interactions[11–13].

In order to form isolated base pairs in the gas phase we desorb a mixture of neat bases from a graphite surface using 10-ns laser pulses at 1,064 nm and at 1 mJ cm^{-2}, followed by entrainment of the neutral, non-fragmented base molecules in a supersonic expansion of argon gas[14]. The expansion lowers the internal temperature of the molecules to a few tens of degrees Kelvin and induces cluster formation. In this way we have formed over 20 different base-pair combinations. By admixing water with the drive gas we can also form clusters of the bases with water molecules, simulating the solvent environment. We have formed such clusters ranging in size from one to fifty water molecules, attached to a single base molecule. We analyse the cold base pairs or clusters downstream with resonance-enhanced multiphoton ionization (REMPI): a photon from a tunable dye laser excites the molecules to the first excited singlet state, whereas a second photon ionizes only those molecules that are excited by the first. We detect the ions in a time-of-flight mass spectrometer. By varying the wavelength we obtain a mass-selected vibronic excitation spectrum. We obtained spectra of all individual bases, of guanine clusters with a single water molecule, and of a variety of base pairs (see Supplementary Information). In order to distinguish different cluster structures we apply spectral hole burning (SHB): while one laser is tuned over all transitions, a second laser, with a 30-ns delay and tuned permanently to a single

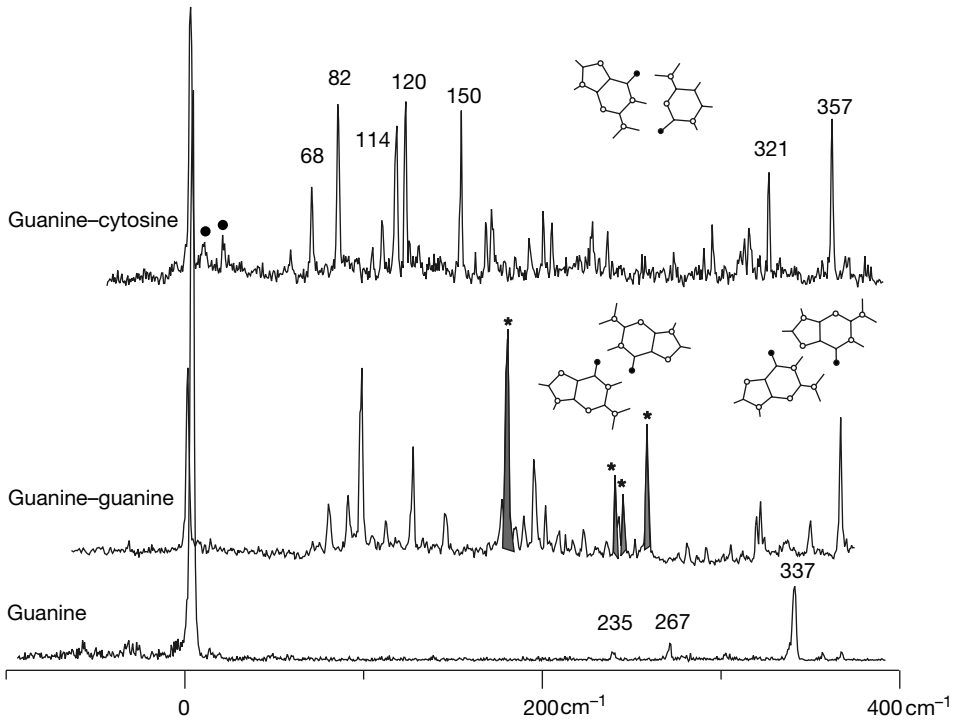

Figure 1 Resonance-enhanced multiphoton ionization (REMPI) spectrum of guanine and its dimers with guanine and cytosine. The spectra are offset such that the origins (0–0 transitions) are shown at the same position for all three species. See text for details.